Optimized Combined Compact Differencing Methods for Computational Aeroacoustics

Ray Hixon*

University of Toledo, Toledo, OH 43606

The sixth order Combined Compact Differencing (CCD) scheme of Chu and Fan is optimized, resulting in exceptional performance. Results indicate that the best of these optimized schemes can accurately propagate linear simple harmonic waves with fewer than three points per wavelength, while using a three point differencing stencil. Stable and accurate boundary treatments for these schemes are given, and the performance of these schemes is assessed using a benchmark problem.

I. Introduction

Computational Aeroacoustics (CAA) is focused on the simulation of acoustic fields produced by unsteady flows.[1–4] To achieve this goal, it is necessary to accurately simulate the unsteady evolution of flow disturbances, which requires the use of high-accuracy spatial and temporal numerical schemes. As these schemes have been developed and validated, the application problems of interest have also increased in complexity, now typically involving realistic nonlinear flows about complex geometries.

The accuracy of the spatial differencing schemes used to evaluate the flux gradients in the governing equations has a major impact on the accuracy of the numerical solution. Two approaches have generally been used to improve the accuracy of the spatial differencing scheme: increasing the order of accuracy of the scheme, or optimizing the wavenumber performance and thus the accuracy of the scheme.

It is important to distinguish between the accuracy and the order of accuracy of a spatial differencing scheme. The accuracy is defined as the error which occurs in a solution when a given grid spacing is used. The order of accuracy is the rate at which the solution error is reduced as the grid spacing is decreased. Thus, two spatial differencing schemes which have the same order of accuracy can give different accuracy on a given grid.

In general, increasing the order of accuracy of a spatial differencing scheme will also improve its accuracy on a given grid. These higher order schemes also have larger stencil sizes, which contributes to accuracy and stability issues near the computational boundaries. For example, a sixth order accurate scheme has a seven point stencil.

The stencil size for a sixth order scheme can be reduced to five points by using a compact differencing scheme, which use both the function and its first derivative values in the differencing stencil.[5,6] These compact schemes also have improved accuracy compared to explicit schemes.

Extending this approach, Chu and Fan proposed a 'combined compact difference' (CCD) scheme, which also incorporates the function second derivative at neighboring points.[7] This results in a three-point stencil, and shows improved accuracy compared to compact schemes.

Another approach for increasing accuracy is to 'optimize' the wavenumber performance of a spatial differencing stencil without increasing the order of accuracy. This approach has been explored by a number of researchers for explicit schemes,[8–10] compact schemes[5,6] and CCD schemes.[11]

In this work, the performance of the Tam and Shen Dispersion Relation Preserving (DRP) scheme,[12] which is a well-known and widely used optimized explicit scheme, is used to guide a new optimization of the CCD scheme. Three optimized schemes are presented, with stable and accurate boundary treatments. The performance of the optimized schemes are verified, and tested using a modified wave propagation test from the ICASE/LaRC Workshop on Benchmark Problems in Computational Aeroacoustics.[13] The results highlight the exceptional performance of the optimized CCD schemes.

*Professor, Mechanical, Industrial, and Manufacturing Engineering (MIME) Department, Senior Member AIAA.

II. Combined Compact Differencing (CCD) Scheme

In this section, the development of the optimized Combined Compact Difference (CCD) scheme is given.

In the optimized CCD scheme, the first $(\widetilde{u}_x)$ and second derivative $(\widetilde{u}_{xx})$ values are calculated at a grid point i using these equations:

$$
\begin{aligned}
(\widetilde{u}_x)_i &= \begin{pmatrix} \frac{a_1}{\Delta x}\left(u_{i+1}-u_{i-1}\right) \\ +b_1\left((\widetilde{u}_x)_{i+1}+(\widetilde{u}_x)_{i-1}\right) \\ +c_1\Delta x\left((\widetilde{u}_{xx})_{i+1}-(\widetilde{u}_{xx})_{i-1}\right) \end{pmatrix} \\
(\widetilde{u}_{xx})_i &= \begin{pmatrix} \frac{a_2}{(\Delta x)^2}\left(u_{i+1}-2u_i+u_{i-1}\right) \\ +\frac{b_2}{\Delta x}\left((\widetilde{u}_x)_{i+1}-(\widetilde{u}_x)_{i-1}\right) \\ +c_2\left((\widetilde{u}_{xx})_{i+1}+(\widetilde{u}_{xx})_{i-1}\right) \end{pmatrix}
\end{aligned} \tag{1}
$$

Here, $(\widetilde{u}_x)$ and $(\widetilde{u}_{xx})$ are the *calculated* values of the function derivatives, not the analytical value.

The CCD scheme requires a block tridiagonal matrix to be solved on each grid line to obtain the calculated derivatives. For example, the matrix equation on a 7-point grid is:

$$
\begin{bmatrix} D_2 & A_2 & 0 & 0 & 0 \\ B_3 & D_3 & A_3 & 0 & 0 \\ 0 & B_4 & D_4 & A_4 & 0 \\ 0 & 0 & B_5 & D_5 & A_5 \\ 0 & 0 & 0 & B_6 & D_6 \end{bmatrix}
\begin{Bmatrix} \partial U_2 \\ \partial U_3 \\ \partial U_4 \\ \partial U_5 \\ \partial U_6 \end{Bmatrix}
=
\begin{Bmatrix} RHS_2 - B_2\partial U_1 \\ RHS_3 \\ RHS_4 \\ RHS_5 \\ RHS_6 - A_6\partial U_7 \end{Bmatrix} \tag{2}
$$

where

$$
\begin{aligned}
\partial U_i &= \begin{Bmatrix} (\widetilde{u}_x)_i \\ (\widetilde{u}_{xx})_i \end{Bmatrix} \\
RHS_i &= \begin{Bmatrix} \frac{a_1}{\Delta x}\left(u_{i+1}-u_{i-1}\right) \\ \frac{a_2}{\Delta x^2}\left(u_{i+1}-2u_i+u_{i-1}\right) \end{Bmatrix}
\end{aligned} \tag{3}
$$

and

$$
\begin{aligned}
B_i &= \begin{bmatrix} -b_1 & c_1\Delta x \\ \frac{b_2}{\Delta x} & -c_2 \end{bmatrix} \\
D_i &= \begin{bmatrix} 1 & 0 \\ 0 & 1 \end{bmatrix} \\
A_i &= \begin{bmatrix} -b_1 & -c_1\Delta x \\ -\frac{b_2}{\Delta x} & -c_2 \end{bmatrix}
\end{aligned} \tag{4}
$$

In this work, the derivatives are optimized for wavenumber performance, and are written as:

$$
\begin{aligned}
(\widetilde{u}_x)_i &= (u_x)_i + \sigma_1(\Delta x)^4(u_{xxxxx})_i + \epsilon_1(\Delta x)^6(u_{xxxxxxx})_i \\
(\widetilde{u}_{xx})_i &= (u_{xx})_i + \sigma_2(\Delta x)^4(u_{xxxxxx})_i + \epsilon_2(\Delta x)^6(u_{xxxxxxxx})_i
\end{aligned} \tag{5}
$$

where σ_1 and σ_2 are the optimization parameters. Note that the CCD method provides two optimization parameters compared to the single optimization parameter used by explicit and compact differencing schemes.

The coefficients of the leading error terms are ϵ_1 and ϵ_2, and are:

$$
\begin{aligned}
\epsilon_1 &= \frac{1}{9450}+\frac{-5\sigma_1+2\sigma_2+360\sigma_1\left(\sigma_2-\sigma_1\right)}{30} \\
\epsilon_2 &= \frac{-\left(\frac{19}{12600}-\frac{11\sigma_1}{14}+\frac{3\sigma_2}{10}-216\sigma_1^2-144\sigma_1\sigma_2-72\sigma_2^2-51480\sigma_1^2\sigma_2+51480\sigma_1\sigma_2^2\right)}{6\left(1-720\sigma_1\right)}
\end{aligned} \tag{6}
$$

The coefficient values are:

$$
\begin{aligned}
a_1 &= \frac{15}{16-720\sigma_1} \\
b_1 &= -\left(\frac{7+360\sigma_1}{16-720\sigma_1}\right) \\
c_1 &= \frac{1+180\sigma_1}{16-720\sigma_1} \\
a_2 &= \frac{24-4320\sigma_1+4320\sigma_2}{8-3600\sigma_1+720\sigma_2} \\
b_2 &= -\left(\frac{9+2160\sigma_2}{8-3600\sigma_1+720\sigma_2}\right) \\
c_2 &= \frac{1+360\sigma_1+360\sigma_2}{8-3600\sigma_1+720\sigma_2}
\end{aligned} \tag{7}
$$

Note that if the values of the optimization parameters are set to zero, the coefficients for the original sixth order CCD scheme of Chu and Fan[7] are obtained. The new optimized scheme is fourth order accurate for any other values of the optimization parameters.

III. Wavenumber Analysis and Optimization

In this section, the wavenumber performance of the CCD scheme is presented and the optimization method is discussed.

III.A. Wavenumber Performance of Numerical Schemes

In order to analyze the performance of the CCD scheme, this model equation is used:

$$
u_t + cu_x - \mu u_{xx} = 0 \tag{8}
$$

with a simple harmonic initial condition:

$$
u\left(x,0\right) = A_0 e^{ikx} \tag{9}
$$

The solution to this equation is:

$$
u\left(x,t\right) = \left(A_0 e^{-\lambda t}\right) e^{i(kx-\omega t)} \tag{10}
$$

where:

$$
\begin{aligned}
\lambda &= \mu k^2 \\
\omega &= ck
\end{aligned} \tag{11}
$$

Thus, as time progresses, the initial wave propagates in the positive x direction at a speed of c while reducing in amplitude at an exponential rate.

When this equation is solved numerically, the numerically computed derivative values will not be correct:

$$\begin{aligned}\widetilde{u}_x &= i\widetilde{k}u \\ \widetilde{u}_{xx} &= -\widetilde{\delta}u\end{aligned} \tag{12}$$

These numerically computed derivatives can be rewritten in terms of the correct analytical derivatives as:

$$\begin{aligned}\widetilde{u}_x &= \frac{\widetilde{k}\Delta x}{k\Delta x}\left(iku\right) \\ \widetilde{u}_{xx} &= \frac{\widetilde{\delta}\Delta x^2}{\left(k\Delta x\right)^2}\left(-k^2u\right)\end{aligned} \tag{13}$$

and, assuming a 'perfect' time integration scheme, the numerical solution to the model equation will be:

$$\widetilde{u}\left(x,t\right) = \left(A_0e^{-\beta\lambda t}\right)e^{i(kx-\alpha\omega t)} \tag{14}$$

where:

$$\begin{aligned}\alpha &= \frac{\widetilde{k}\Delta x}{k\Delta x} \\ \beta &= \frac{\widetilde{\delta}\Delta x^2}{\left(k\Delta x\right)^2}\end{aligned} \tag{15}$$

Thus, in the numerical solution, the simple harmonic wave will propagate as if the speed had a different value (known as 'dispersion error'):

$$\widetilde{c} = \alpha c$$

and will damp as if the viscosity had a different value (known as 'dissipation error'):

$$\widetilde{\mu} = \beta\mu$$

In the next section, the CCD scheme will be optimized to reduce these dispersion and dissipation errors to an acceptable level over the widest range of $(k\Delta x)$ values possible.

III.B. Numerical Wavenumber of CCD Scheme

Substituting the simple harmonic function into the CCD equations to determine the numerical derivatives gives:

$$\begin{aligned}i\widetilde{k}u_i &= i\widetilde{k}b_1\left(e^{ik\Delta x}+e^{-ik\Delta x}\right)u_i - \widetilde{\delta}c_1\Delta x\left(e^{ik\Delta x}-e^{-ik\Delta x}\right)u_i + \frac{a_1}{\Delta x}\left(e^{ik\Delta x}-e^{-ik\Delta x}\right)u_i \\ -\widetilde{\delta}u_i &= i\widetilde{k}\frac{b_2}{\Delta x}\left(e^{ik\Delta x}-e^{-ik\Delta x}\right)u_i - \widetilde{\delta}c_2\left(e^{ik\Delta x}+e^{-ik\Delta x}\right)u_i + \frac{a_2}{\Delta x^2}\left(e^{ik\Delta x}-2+e^{-ik\Delta x}\right)u_i\end{aligned} \tag{16}$$

This results in a matrix equation, which can be solved to obtain:

$$\left\{\begin{array}{c}\left(\widetilde{k}\Delta x\right) \\ \left(\widetilde{\delta}\Delta x^2\right)\end{array}\right\} = \frac{1}{\left(\begin{array}{c}-1-4b_2c_1 \\ +2\left(b_1+c_2\right)\cos\left(k\Delta x\right) \\ -4\left(b_1c_2-b_2c_1\right)\cos^2\left(k\Delta x\right)\end{array}\right)}\left\{\begin{array}{c}\left(\begin{array}{c}4\left(a_1c_2-a_2c_1\right)\cos\left(k\Delta x\right)\sin\left(k\Delta x\right) \\ +2\left(2a_2c_1-a_1\right)\sin\left(k\Delta x\right)\end{array}\right) \\ \left(\begin{array}{c}4\left(a_1b_2-a_2b_1\right)\cos^2\left(k\Delta x\right) \\ +2\left(2a_2b_1+a_2\right)\cos\left(k\Delta x\right) \\ -2\left(2a_1b_2+a_2\right)\end{array}\right)\end{array}\right\} \tag{17}$$

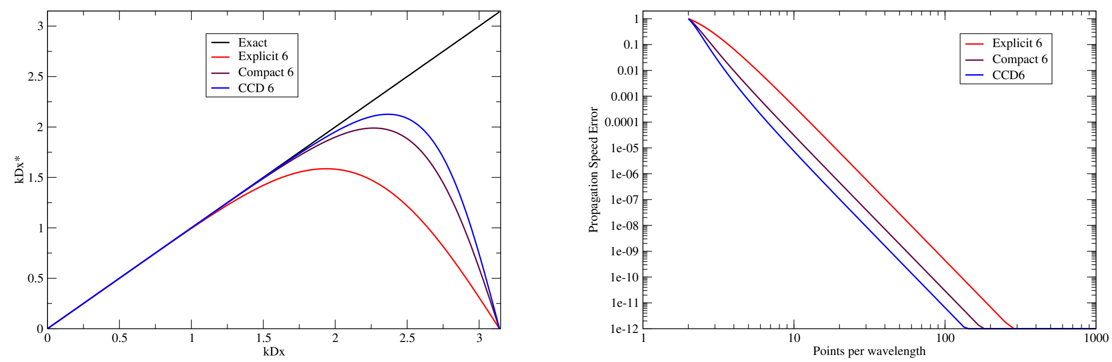

a **b**

Figure 1. Comparison of Sixth Order Scheme Performance (a: Numerical Wavenumber, b: Propagation Speed Error)

Figure 1 compares the numerical wavenumbers $\left(\widetilde{k}\Delta x\right)$ and wavenumber ratio error $|1-\alpha|$ for the sixth order explicit, compact, and CCD ($\sigma_1 = \sigma_2 = 0$) first derivatives.

In these figures, the number of grid points per wavelength (PPW) is defined as:

$$PPW = \frac{2\pi}{k\Delta x} \tag{18}$$

These figures show the exceptional performance of the sixth order CCD scheme compared to the explicit and compact schemes with sixth order accuracy.

III.C. Optimized CCD Schemes

The CCD scheme was then optimized to improve performance, using Eq. (17) to define the numerical wavenumber of the optimized CCD scheme. Three optimization cases were considered:

- kDX Opt: Obtain the best wave propagation performance (α) result with no consideration of the accuracy of the dissipation performance (β).
- dDX2 Opt: Obtain the best dissipation performance (β) result with no consideration of the wave propagation performance (α). .
- Blended Opt: Obtain the best result for *both* wave propagation performance (α) *and* dissipation performance (β). To accomplish this, the 'worst case' between α and β was used to define the measure of accuracy .

The initial values for σ_1 and σ_2 were determined for each of the three optimization cases using a 'brute force' approach. A 1001 x 1001 point (σ_1, σ_2) grid was defined over the range

$$\begin{aligned} -0.002 \leq \quad & \sigma_1 \quad \leq 0.002 \\ -0.0006 \leq \quad & \sigma_2 \quad \leq 0.0006 \end{aligned} \tag{19}$$

For each grid point, Eqn. (17) was used to determine the lowest value of $(k\Delta x)$ where the appropriate α or β accuracy limit was reached (using the Tam and Shen DRP scheme as a guide to choose the accuracy limit value of 0.001):

$$\begin{aligned} |1-\alpha| \quad & > \quad 0.001 \\ |1-\beta| \quad & > \quad 0.001 \end{aligned} \tag{20}$$

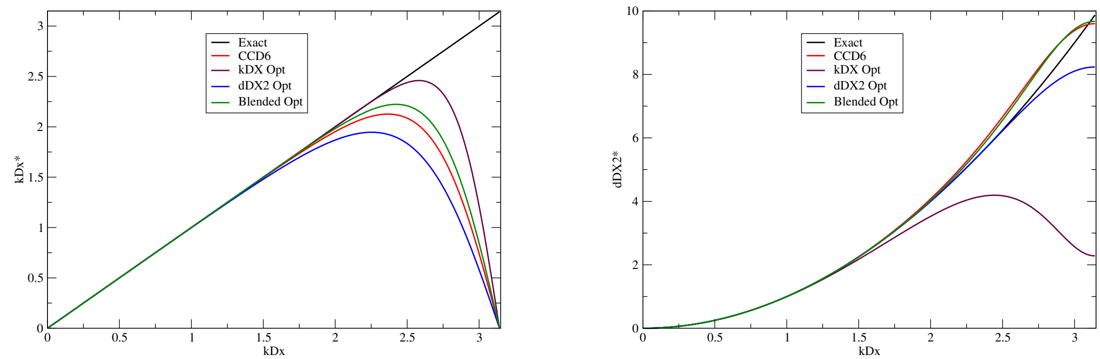

a **b**

Figure 2. Wavenumber Comparison of Optimized CCD Schemes (a: Dispersion, b: Dissipation)

The $(k\Delta x)$ values where the accuracy limit was reached were denoted as $(k\Delta x)_\alpha$ and $(k\Delta x)_\beta$, respectively.

The results of the three optimization cases are given in Table 1.

Figures 2-4 compare the performance of the optimized schemes to the original CCD6 scheme. The effect of the optimization, as well as the clearly improved performance of the optimized schemes, is clearly seen in the figures.

Figure 2 shows the effect of the three optimizations on the numerical dispersion and dissipation performance of the CCD schemes. This figure highlights the differences in the three new schemes, and the enhanced dispersion or dissipation performance.

Figure 3 illustrates that the 'kDX Opt' optimization is focused on keeping the value of α between 0.999 and 1.001 as long as possible, and shows the equivalent 'dDX2 Opt' optimization for β. In both plots, the 'Blended Opt' optimization is less aggressive on either α or β; instead, it obtains the best minimum value of the accuracy limit for either.

Figure 4 highlights the practical results of this optimization. In these graphs, it is clearly seen that the optimization reduces the error below 0.001 to a lower value of grid points per wavelength – allowing an accurate solution to be obtained with fewer grid points.

However, this improved performance is at the cost of a lower order of accuracy. In figure 4 , the order of accuracy of the scheme is directly related to the slope of the error curve at high values of points per wavelength. The reduced order of accuracy of the optimized schemes is clearly shown when compared to the original CCD6 scheme. The scheme user must decide whether the reduced order of accuracy is an acceptable price to pay for the improved accuracy at low points per wavelength.

IV. Boundary Stencils and Scheme Verification

In this section, the boundary stencils, scheme verification, and linear stability results are presented.

Case	σ_1	σ_2	$(k\Delta x)_\alpha$	$(k\Delta x)_\beta$	$\left(\widetilde{k}\Delta x\right)_{max}$	$\left(\widetilde{\delta}\Delta x^2\right)_{max}$
CCD6	0.0	0.0	1.32 (PPW = 4.76)	1.24 (PPW = 5.07)	2.17	9.60
kDX Opt	-0.000568	-0.005664	2.27 (PPW = 2.77)	0.643 (PPW = 9.77)	2.46	4.12
dDX2 Opt	-0.001668	-0.000540	0.849 (PPW = 7.40)	2.42 (PPW = 2.60)	1.95	8.24
Blended Opt	0.000316	-0.000780	1.76 (PPW = 3.57)	1.74 (PPW = 3.61)	2.23	9.67

Table 1. Optimization Results

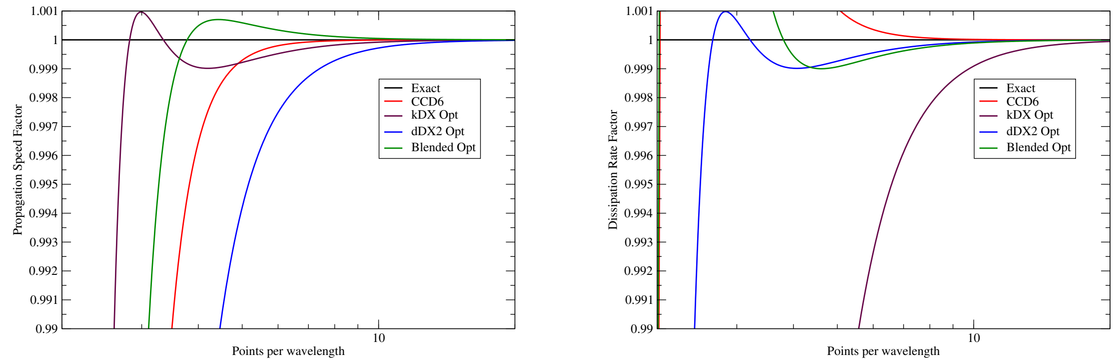

a **b**

Figure 3. Performance Comparison of Optimized CCD Schemes (a: Propagation Speed, b: Dissipation Rate)

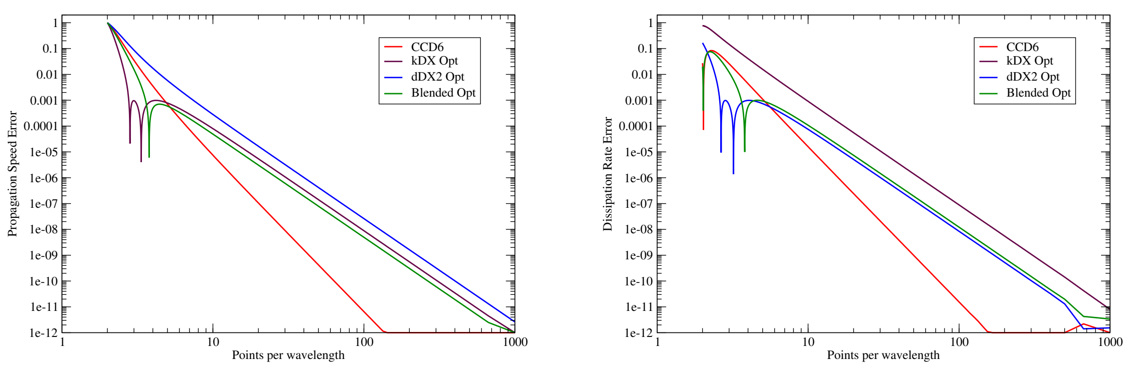

a **b**

Figure 4. Performance Comparison of Optimized CCD Schemes (a: Propagation Speed Error, b: Dissipation Rate Error)

IV.A. Boundary stencils

For ease of boundary condition imposition, explicit boundary stencils are used. The Hixon et al. 'ghost point' method[14] is used to impose the boundary condition; this method has proved to be stable for high-order schemes up to sixth order accuracy. This method is notable because the boundary condition affects the derivative values at the boundary point and its two neighboring grid points, due to the large differencing stencils used.

Three boundary treatment methods were tested:

- The **b1** method uses one 7-point explicit stencil at each boundary, which matches the first six CCD Taylor series terms. This method uses the least number of explicit boundary stencils, but requires the CCD derivatives to be updated throughout the domain when boundary derivative corrections are imposed.

- The **b4** method uses four 7-point explicit stencils at each boundary, which match the first six CCD Taylor series terms. This method does not require the CCD derivatives to be updated when boundary derivative corrections are imposed, since the fourth explicit stencil does not use the ghost point.

- The **b5** method uses five explicit stencils at each boundary. The first four stencils are identical to the **b4** stencils, while the fifth stencil uses a 9 point central difference designed to match the first *eight*

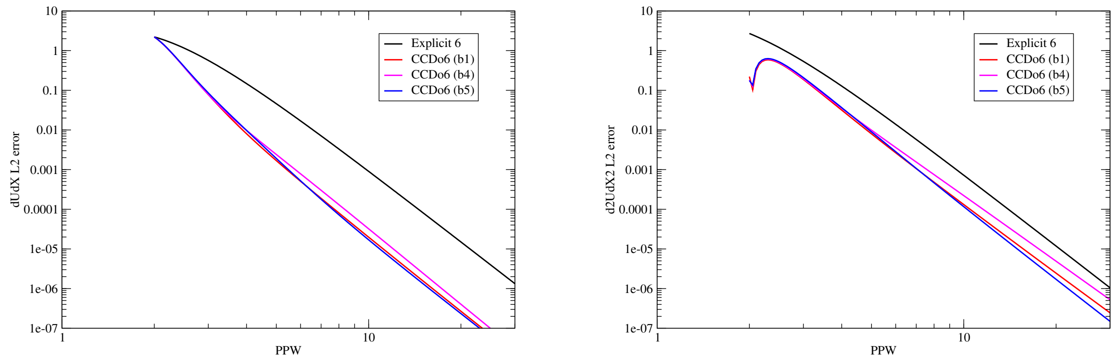

a **b**

Figure 5. Effect of Sixth Order CCD Scheme Boundary Stencils on L2 Error (a: First Derivative , b: Second Derivative)

terms of the CCD differencing scheme (which includes the leading error term of the CCD scheme). This method also does not require the CCD derivatives to be updated when boundary derivative corrections are imposed.

Note that both first and second derivative stencils are required for the CCD scheme. The boundary stencils and correction coefficients are given in Appendix A.

IV.B. Verification of Numerical Schemes

As a test of their actual performance, the unoptimized CCD scheme and the three optimized CCD schemes were used to calculate the derivatives of the function:

$$f\left(x\right) = \sin\left(\pi x + \frac{\pi}{4}\right), \quad 0 \leq x \leq 20$$

For these tests, there were 20 wavelengths in the computational domain. A range of grid densities (from 41 to 1041) was used in the computational domain. An additional five grid points were added at each end of the grid; the results at these point were not used in the error calculations.

Figure 5 shows the effect of the boundary stencils on the unoptimized CCD scheme results. There are visible differences, particularly in the results for the second derivatives. In all cases, the **b5** boundary treatment is the most accurate.

Figure 6 shows the computed order of accuracy for these results. This figure clearly shows that the **b5** boundary treatment is obtaining the design order of accuracy, and the **b1** and **b4** boundary treatments are not.

Upon further investigation, it was determined that the value of the leading error term of the **b1** and **b4** boundary stencils was different than that of the interior CCD scheme, and that this was causing the calculated CCD second derivative values to lose one order of accuracy near the boundaries. This loss of accuracy was clearly seen in the second derivative L2 errors.

This loss of formal order of accuracy near the boundary has previously reported for the case of Runge-Kutta time marching schemes applied to unsteady CAA calculations.[15] When a function is repeatedly differentiated numerically, a loss of accuracy occurs when the leading error terms of neighboring differencing stencils do not match. *This occurs in both CCD derivative equations, but is most noticeable in the second derivative results.*

While all three boundary treatments were found to be linearly stable, the **b5** treatment is most accurate. From this point, only the **b5** results will be shown.

Figures 7 and 8 show the **b5** results for all of the CCD schemes. Figure 7 clearly shows the reduced error at low points per wavelength (PPW) due to the optimization, and also clearly shows the reduced convergence rate as the number of points per wavelength increases. Figure 8 confirms that the optimized schemes have been reduced from sixth order accuracy to fourth order accuracy.

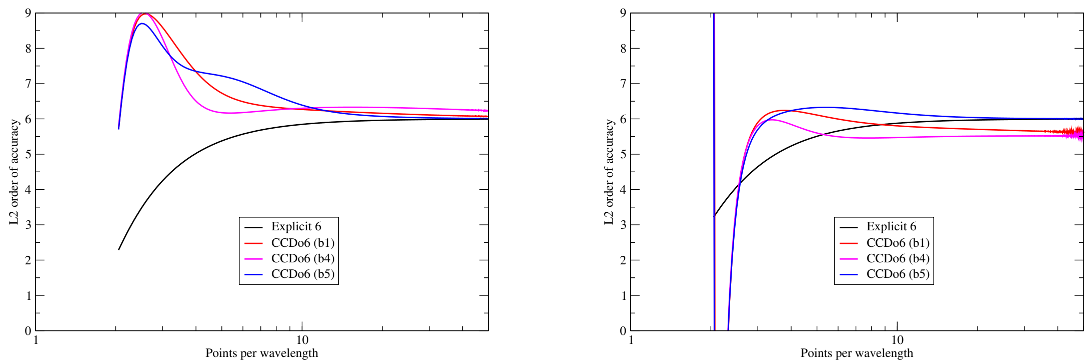

a b

Figure 6. Effect of Sixth Order CCD Scheme Boundary Stencils on Order of Accuracy (a: First Derivative , b: Second Derivative)

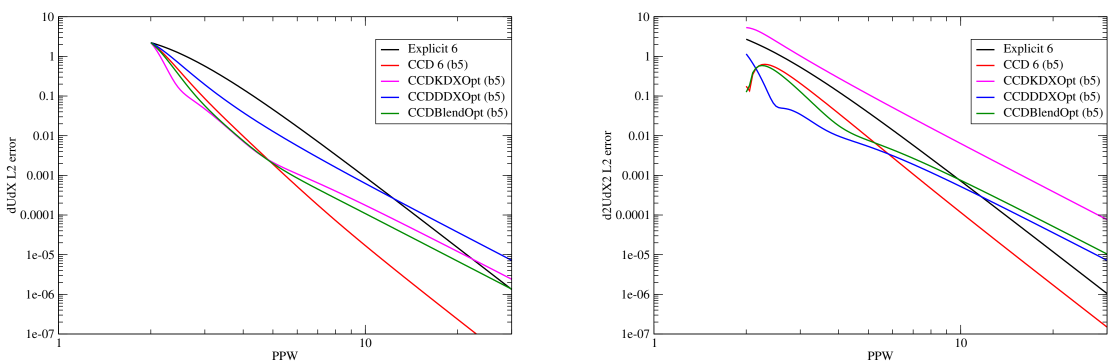

a b

Figure 7. Effect of CCD Scheme Optimization on L2 Error (a: First Derivative , b: Second Derivative)

IV.C. Linear Stability

The linear stability of all CCD schemes was verified for both propagation and dissipation, using a 101 x 101 matrix. Three conditions were assessed:

- Wave propagation, using the linear advection equation with zero incoming wave amplitude.
- Dissipation, using the heat equation with specified temperature at the boundaries.
- Dissipation, using the heat equation with specified temperature derivatives at the boundaries.

Figure 9 shows the computed eigenvalues for the CCD schemes using the **b5** boundary treatment. The stability of the CCD schemes for both propagation and dissipation is clearly shown.

V. Numerical Tests

In this section, the Category 1 Problem 1 benchmark problem from the First CAA Workshop[13] is used to assess the performance and long-time stability of the optimized CCD schemes. No artificial dissipation was added to the scheme for these tests.

In this problem, the linear advection equation is solved:

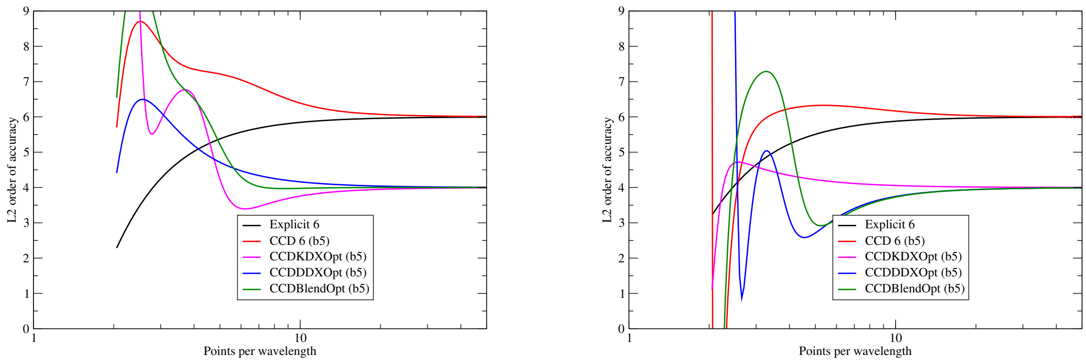

a **b**

Figure 8. Effect of CCD Scheme Optimization on Order of Accuracy (a: First Derivative , b: Second Derivative)

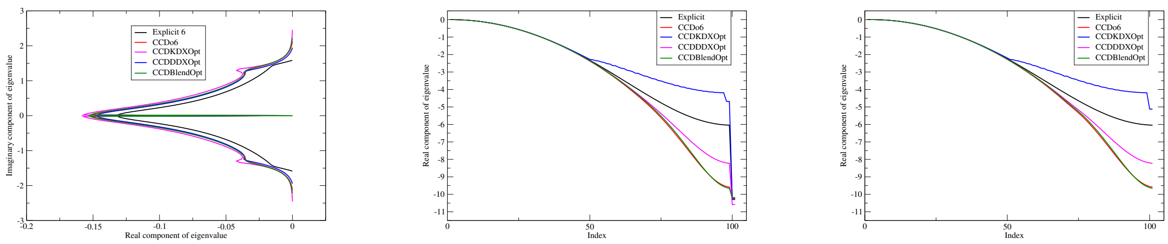

a **b** **c**

Figure 9. Linear Stability of Optimized CCD Schemes (a: Propagation , b: Specified Boundary Value Dissipation, c: Specified Boundary Derivative Dissipation)

$$\frac{\partial u}{\partial t} + \frac{\partial u}{\partial x} = 0$$

The initial condition is:

$$u(x,0) = \frac{1}{2} e^{-\ln 2 \left(\frac{x}{3}\right)^2}$$

The computational domain was extended upstream to avoid problems from the initial condition:

$$-50 \leq x \leq 450$$
$$\Delta x = 1$$

The Stanescu and Habashi 2N-storage[16] form of Hu et al.'s 5-6 Low-Dissipation and Low-Dispersion Runge-Kutta (LDDRK) scheme[17] was used for time marching. Tests showed that the errors from the time marching scheme dominated the computed solutions when too large of a time step was used; a CFL condition of 0.1 was used to minimize this issue.

Figure 10 shows the computed solution at time = 400 and the long-term L2 error from the CCD schemes for this case. In this figure, all of the CCD schemes except for the DDXOpt scheme are performing very well. It is noted that the DDXOpt scheme is optimized for dissipation, and is not expected to perform well for this dispersion-dominated test case.

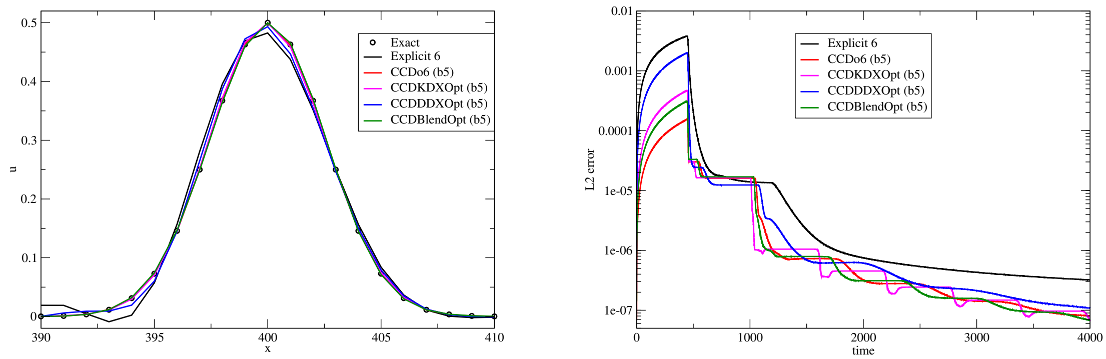

a **b**

Figure 10. Comparison of CCD Scheme Performance on CAA Benchmark Problem (a: Solution at t = 400, b: L2 error history

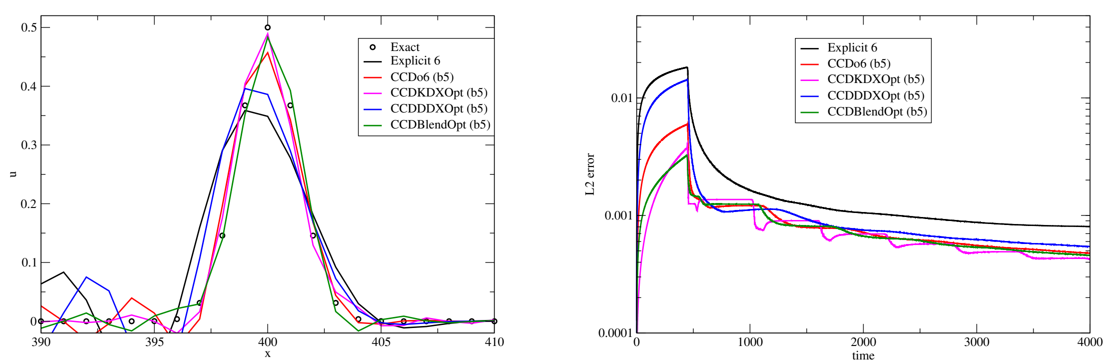

a **b**

Figure 11. Comparison of CCD Scheme Performance on Modified CAA Benchmark Problem (a: Solution at t = 400, b: L2 error history

The L2 error plots show that the errors due to the incorrect numerical propagation speed continuously grow until time = 450, when the wave propagates out of the domain and leaves a quiescent medium behind. The L2 error then drops by several orders of magnitude as spurious waves continue to escape through the boundaries.

It is interesting to note that the unoptimized CCD scheme has the lowest L2 error in this test; this is because the initial wave is very well resolved by all CCD schemes.

In order to confirm this, the initial condition was changed to a Gaussian with a much smaller half-width:

$$u(x,0) \quad = \quad \frac{1}{2}e^{-\ln 2\left(\frac{x}{1.5}\right)^2}$$

Figure 11 shows the computed solution at time = 400 and the long-term L2 error from the CCD schemes for the modified case. In this figure, noticeable differences are seen in the performance of the CCD schemes, with the optimized schemes performing noticeably better than the unoptimized CCD scheme. Again, the DDXOpt scheme has the worst performance of the CCD schemes.

The L2 error plots show that the errors due to the incorrect numerical propagation speed continuously grow until time = 450, when the wave propagates out of the domain and leaves a quiescent medium behind. The L2 error then drops as spurious waves continue to escape through the boundaries, showing the stability of the CCD schemes even with high-wavenumber solution components in the computational domain.

In the modified case, the optimized CCD schemes have the lowest L2 errors while the wave is in the computational domain. This illustrates the advantages of the optimized schemes when there are marginally-resolved waves in the domain.

VI. Conclusions

In this work, the Combined Compact Differencing (CCD) scheme of Chu and Fan was optimized for improved performance at very low grid densities. Three boundary treatments were developed and tested for accuracy and stability, with a new type of boundary treatment that matches the leading error term of the CCD scheme showing the best performance.

The resulting schemes are robust and show exceptional performance on a widely-used benchmark CAA problem. These schemes represent the current state of the art in computational aeroacoustics, and have the potential to further reduce the number of grid points by an order of magnitude for three dimensional problems compared to existing CAA schemes.

Acknowledgments

This work was supported by the NASA Advanced Air Transport Technology (AATT) Project. The author would like to thank Dr. Edmane Envia of the NASA Glenn Research Center, who was the technical monitor for this work.

References

[1] Tam, C. K. W., "Computational Aeroacoustics: Issues and Methods," *AIAA J.*, Vol. 33, 1995, pp. 1788–1796.

[2] Lele, S. K., "Computational Aeroacoustics: A Review," *AIAA Paper 97-0018*, January 1997.

[3] Tam, C. K. W., "Computational Aeroacoustics: An Overview of Computational Challenges and Applications," *Int. J. Comp. Fluid Dyn.*, Vol. 18, 2004, pp. 547–567.

[4] Colonius, T. and Lele, S. K., "Computational Aeroacoustics: Progress in Nonlinear Problems of Sound Generation," *Prog. Aero. Sci.*, Vol. 40, 2004, pp. 345–416.

[5] Lele, S. K., "Compact Finite-Difference Schemes with Spectral-Like Resolution," *J. Comp. Phys.*, Vol. 103, 1992, pp. 16–42.

[6] Kim, J. W. and Lee, D. J., "Optimized compact finite difference schemes with maximum resolution," *AIAA J.*, Vol. 34, 1996, pp. 887–893.

[7] Chu, P. C. and Fan, C., "A three-point combined compact difference scheme," *J. Comp. Phys.*, Vol. 140, 1998, pp. 370–399.

[8] Tam, C. K. W. and Webb, J. C., "Dispersion-Relation-Preserving Finite Difference Schemes for Computational Aeroacoustics," *J. Comp. Phys.*, Vol. 107, 1993, pp. 262–281.

[9] Zingg, D. W., Lomax, H., and Jurgens, H. M., "An Optimized Finite-Difference Scheme for Wave Propagation Problems," *AIAA Paper 1993-0459*, January 1993.

[10] Haras, Z. and Ta'asan, S., "Finite-Difference Schemes for Long-Time Integration," *J. Comp. Phys.*, Vol. 114, 1994, pp. 265–279.

[11] Sengupta, T. K., Lakshmanan, V., and Vijay, V. V. S. N., "A new combined stable and dispersion relation preserving compact scheme for non-periodic problems," *J. Comp. Phys.*, Vol. 228, 2009, pp. 3048–3071.

[12] Tam, C. K. W. and Shen, H., "Direct Computation of Nonlinear Acoustic Pulses Using High-Order Finite Difference Schemes," *AIAA Paper 1993-4325*, 1993.

[13] Hardin, J. C., Ristorcelli, J. R., and Tam, C. K. W., editors, *ICASE/LaRC Workshop on Benchmark Problems in Computational Aeroacoustics (CAA)*, NASA Conference Publication 3300, May 1995.

[14] Hixon, R., Nallasamy, M., and Sawyer, S., "A method for the Implementation of Boundary Conditions in High-Accuracy Finite-Difference Schemes," *AIAA Paper 2005-0608*, January 2005.

[15] Hixon, R., "On the Accuracy of Boundary Stencils for Runge-Kutta Time Marching Schemes," *AIAA Paper 2017-3177*, June 2017.

[16] Stanescu, D. and Habashi, W. G., "2N-storage low dissipation and dispersion Runge-Kutta schemes for computational acoustics," *J. Comp. Phys.*, Vol. 143, 1998, pp. 674–681.

[17] Hu, F. Q., Manthey, J. L., and Hussaini, M. Y., "Low-dissipation and low-dispersion Runge-Kutta schemes for computational acoustics," *J. Comp. Phys.*, Vol. 124, No. 1, 3 1996.

Appendix A: Boundary Treatments

In this Appendix, the boundary stencils and corrections are given for the $i = 1$ boundary; the corresponding stencils for the $i = iMax$ boundary are straightforward to obtain.

Ghost Point Initialization

The ghost point initialization is:

$$f_{GPT} = 7f_1 - 21f_2 + 35f_3 - 35f_4 + 21f_5 - 7f_6 + f_7$$

Boundary Stencils

The boundary stencils are:

$$\left.\frac{\partial f}{\partial x}\right|_{i=1} = \left(\frac{1}{60\Delta x}\right)\begin{pmatrix} -(10+150\sigma_1)\,f_{GPT} \\ -(77-840\sigma_1)f_1 \\ +(150-1950\sigma_1)f_2 \\ -(100-2400\sigma_1)f_3 \\ +(50-1650\sigma_1)f_4 \\ -(15-600\sigma_1)f_5 \\ +(2-90\sigma_1)f_6 \end{pmatrix}$$

$$\left.\frac{\partial^2 f}{\partial x^2}\right|_{i=1} = \left(\frac{1}{180\Delta x^2}\right)\begin{pmatrix} (137+180\sigma_2)f_{GPT} \\ -(147+1080\sigma_2)f_1 \\ -(255-2700\sigma_2)f_2 \\ +(470-3600\sigma_2)f_3 \\ -(285-2700\sigma_2)f_4 \\ +(93-1080\sigma_2)f_5 \\ -(13-180\sigma_2)f_6 \end{pmatrix}$$

$$\left.\frac{\partial f}{\partial x}\right|_{i=2} = \left(\frac{1}{60\Delta x}\right)\begin{pmatrix} (2-90\sigma_1)f_{GPT} \\ -(24-480\sigma_1)f_1 \\ -(35+1050\sigma_1)f_2 \\ +(80+1200\sigma_1)f_3 \\ -(30+750\sigma_1)f_4 \\ +(8+240\sigma_1)f_5 \\ -(1+30\sigma_1)f_6 \end{pmatrix}$$

$$\left.\frac{\partial^2 f}{\partial x^2}\right|_{i=2} = \left(\frac{1}{180\Delta x^2}\right)\begin{pmatrix} -(13-180\sigma_2)f_{GPT} \\ +(228-1080\sigma_2)f_1 \\ -(420-2700\sigma_2)f_2 \\ +(200-3600\sigma_2)f_3 \\ +(15+2700\sigma_2)f_4 \\ -(12+1080\sigma_2)f_5 \\ +(2+180\sigma_2)f_6 \end{pmatrix}$$

$$\left.\frac{\partial f}{\partial x}\right|_{i=3} = \left(\frac{1}{60\Delta x}\right)\begin{pmatrix} -(1+30\sigma_1)f_{GPT} \\ +(9+120\sigma_1)f_1 \\ -(45+150\sigma_1)f_2 \\ +(45+150\sigma_1)f_4 \\ -(9+120\sigma_1)f_5 \\ +(1+30\sigma_1)f_6 \end{pmatrix}$$

$$\left.\frac{\partial^2 f}{\partial x^2}\right|_{i=3} = \left(\frac{1}{180\Delta x^2}\right)\begin{pmatrix} (2+180\sigma_2)f_{GPT} \\ -(27+1080\sigma_2)f_1 \\ +(270+2700\sigma_2)f_2 \\ -(490+3600\sigma_2)f_3 \\ +(270+2700\sigma_2)f_4 \\ -(27+1080\sigma_2)f_5 \\ +(2+180\sigma_2)f_6 \end{pmatrix}$$

$$\left.\frac{\partial f}{\partial x}\right|_{i=4} = \left(\frac{1}{60\Delta x}\right)\begin{pmatrix} -(1+30\sigma_1)f_1 \\ +(9+120\sigma_1)f_2 \\ -(45+150\sigma_1)f_3 \\ +(45+150\sigma_1)f_5 \\ -(9+120\sigma_1)f_6 \\ +(1+30\sigma_1)f_7 \end{pmatrix}$$

$$\left.\frac{\partial^2 f}{\partial x^2}\right|_{i=4} = \left(\frac{1}{180\Delta x^2}\right)\begin{pmatrix} (2+180\sigma_2)f_1 \\ -(27+1080\sigma_2)f_2 \\ +(270+2700\sigma_2)f_3 \\ -(490+3600\sigma_2)f_4 \\ +(270+2700\sigma_2)f_5 \\ -(27+1080\sigma_2)f_6 \\ +(2+180\sigma_2)f_7 \end{pmatrix}$$

$$\left.\frac{\partial f}{\partial x}\right|_{i=5} = \left(\frac{1}{840\Delta x}\right)\begin{pmatrix} (3+140\sigma_1-420\epsilon_1)f_1 \\ -(32+1260\sigma_1-2520\epsilon_1)f_2 \\ +(168+3640\sigma_1-5880\epsilon_1)f_3 \\ -(672+4060\sigma_1-5880\epsilon_1)f_4 \\ +(672+4060\sigma_1-5880\epsilon_1)f_6 \\ -(168+3640\sigma_1-5880\epsilon_1)f_7 \\ +(32+1260\sigma_1-2520\epsilon_1)f_8 \\ -(3+140\sigma_1-420\epsilon_1)f_9 \end{pmatrix}$$

$$\left.\frac{\partial^2 f}{\partial x^2}\right|_{i=5} = \left(\frac{1}{5040\Delta x^2}\right)\begin{pmatrix} -(9+1260\sigma_2-5040\epsilon_2)f_1 \\ +(128+15120\sigma_2-40320\epsilon_2)f_2 \\ -(1008+65520\sigma_2-141120\epsilon_2)f_3 \\ +(8064+146160\sigma_2-282240\epsilon_2)f_4 \\ -(14350+189000\sigma_2-352800\epsilon_2)f_5 \\ +(8064+146160\sigma_2-282240\epsilon_2)f_6 \\ -(1008+65520\sigma_2-141120\epsilon_2)f_7 \\ +(128+15120\sigma_2-40320\epsilon_2)f_8 \\ -(9+1260\sigma_2-5040\epsilon_2)f_9 \end{pmatrix}$$

Derivative corrections

The correction to the initial ghost point value (due to a boundary condition) is found as:

$$\Delta f_{GPT} = \frac{60\Delta x}{-(10+150\sigma_1)}\left(\Delta\frac{\partial f}{\partial x}\right)_{BC}$$

or

$$\Delta f_{GPT} = \frac{180\Delta x^2}{137+180\sigma_2}\left(\Delta \frac{\partial^2 f}{\partial x^2}\right)_{BC}$$

where the boundary condition is used to determine a 'correction' to the value of one of the boundary derivatives. See Hixon et al.[14] for a more comprehensive explanation of this process.

This result is used to find the additional boundary derivative corrections:

$$\begin{aligned}
\left(\Delta \frac{\partial f}{\partial x}\right)_{i=1} &= \frac{-(10+150\sigma_1)}{60\Delta x}\Delta f_{GPT} \\
\left(\Delta \frac{\partial^2 f}{\partial x^2}\right)_{i=1} &= \frac{137+180\sigma_2}{180\Delta x^2}\Delta f_{GPT} \\
\left(\Delta \frac{\partial f}{\partial x}\right)_{i=2} &= \frac{2-90\sigma_1}{60\Delta x}\Delta f_{GPT} \\
\left(\Delta \frac{\partial^2 f}{\partial x^2}\right)_{i=2} &= \frac{-(12-180\sigma_2)}{180\Delta x^2}\Delta f_{GPT} \\
\left(\Delta \frac{\partial f}{\partial x}\right)_{i=3} &= \frac{-(1+30\sigma_1)}{60\Delta x}\Delta f_{GPT} \\
\left(\Delta \frac{\partial^2 f}{\partial x^2}\right)_{i=3} &= \frac{2+180\sigma_2}{180\Delta x^2}\Delta f_{GPT} \\
\left(\Delta \frac{\partial f}{\partial x}\right)_{i=4} &= 0 \\
\left(\Delta \frac{\partial^2 f}{\partial x^2}\right)_{i=4} &= 0 \\
\left(\Delta \frac{\partial f}{\partial x}\right)_{i=5} &= 0 \\
\left(\Delta \frac{\partial^2 f}{\partial x^2}\right)_{i=5} &= 0
\end{aligned}$$

To be clear: any boundary condition imposed on either the first or second derivative at the boundary will have an effect on *both* derivatives at the boundary ($i = 1$). In addition, the boundary condition affects the derivatives at the $i = 2$ and $i = 3$ grid points (but not the $i = 4$ or $i = 5$ grid points, because the ghost point value is not used to calculate these derivatives). The same is true at the $i = iMax$ boundary.